Inorganic Chemistry

Article

pubs.acs.org/IC

$Na_2CaSn_2Ge_3O_{12}$: A Novel Host Lattice for Sm^{3+}-Doped Long-Persistent Phosphorescence Materials Emitting Reddish Orange Light

Jiao Xu, Zhenghua Ju, Xiuping Gao, Yanqing An, Xiaoliang Tang, and Weisheng Liu*

Key Laboratory of Nonferrous Metals Chemistry, Resources Utilization of Gansu Province, and State Key Laboratory of Applied Organic Chemistry, College of Chemistry and Chemical Engineering, Lanzhou University, Lanzhou 730000, People's Republic of China

Supporting Information

ABSTRACT: A novel host lattice disodium calcium ditin(IV) trigermanium oxide $Na_2CaSn_2Ge_3O_{12}$ was utilized for synthesizing long-persistent phosphorescence materials for the first time. Reddish orange long-persistent phosphorescence was observed in $Na_2CaSn_2Ge_3O_{12}$:Sm^{3+} phosphors with persistence time more than 4.8 h. The phosphors were synthesized by a conventional solid-state reaction pathway in air atmosphere. A predominant cubic phase of $Na_2CaSn_2Ge_3O_{12}$ was observed in all XRD patterns. Photoluminescence measurements indicated that the emission spectrum was composed of the peaks located at 566 (the strongest), 605, 664, and 724 nm. The results of the decay curves in terms of a biexponential model suggest that different defects appear in the crystal lattice. The defects acting as traps were investigated by thermoluminescence, which demonstrated that doping Sm^{3+} ions into the $Na_2CaSn_2Ge_3O_{12}$ host has made the trap types abundant. Furthermore, the origin of the long-persistent phosphorescence has also been discussed. On the basis of the above results, Sm^{3+}-doped $Na_2CaSn_2Ge_3O_{12}$ phosphors are considered to have potential practical applications.

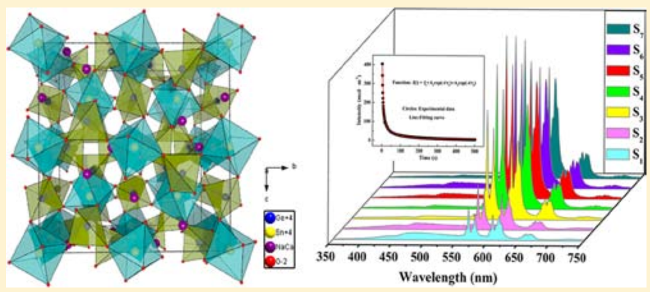

■ INTRODUCTION

Long-persistent phosphorescence (LPP) materials can store the absorbed light energy and release it in the form of luminescence after stoppage of the excitation.[1−3] Recently, great attention has been attracted to design and construct new excellent LPP phosphors which are potentially applied in the fields such as safety indication, detection of high-energy rays, road signs, automobile instruments, and so on.[3−6] In theory, different color-emitting LPPs can be obtained through mixing the three primary colors (blue, green, and red) emitting LPPs with similar properties (chemical and physical) at = proper proportion.[6] LPP phosphors for two of the tricolor, blue[7] and green,[4] which possess high brightness, long persistent time, and good chemical stability, are commercially available. However, the luminosity, and/or the duration time of the LPP materials which emit in the long wavelength (orange to red) region still cannot meet the needs of commercial application.[8] Furthermore, considering the biomedical research and medicine applications, the emission wavelength at the longer region from 650 nm to the infrared is more suitable for use as luminescent probes for in vivo imaging.[9] Hence, there is a strong desire for exploring excellent reddish orange LPP.

In the earlier times of this research, divalent europium ion (Eu^{2+}) activated sulfides such as MS:Eu^{2+} (M = Ca, Sr)[10,11] were used to prepare red LPP phosphors, but they are chemically unstable and sensitive to moisture. Diallo et al. developed a new red LPP phosphor $CaTiO_3$:Pr^{3+}. The afterglow time of the phosphor is too short, although it is approximately ideal red.[12] Murazaki et al. reported a red LPP phosphor Y_2O_2S:Eu^{3+},Mg^{2+},Ti^{4+}, which shows a longer red afterglow time. The S as a sulfurization agent in the process is harmful to environment.[13] In recent years, red LPP of MO:Eu^{3+} (M = Ca, Sr, and Ba)[14] and M_2SnO_4:Sm^{3+} (M = Ca, Sr, and Ba)[15−17] were reported. But, so far, no perfect red or reddish orange LPP phosphor has been obtained in practical application.

Theoretically, the occurrence of LPP relies on two kinds of active centers which exist in phosphors, emitters, and traps. Emitters can emit radiation after being excited. Traps with suitable depth are able to store excitation energy and immobilize it for an appropriately long time, and then release and transfer it to the emitters by degrees as a result of external thermal stimulations.[18] The emission wavelength of LPP mainly depends on the emitter, while the afterglow intensity and duration time are depending on the property of the trap. Therefore, a proper emitter which is capable of emitting reddish orange light and a suitable host which is able to create appropriate traps and generate persistent luminescence are required in designing reddish orange LPP phosphors. Among

Received: May 20, 2013
Published: November 21, 2013

dx.doi.org/10.1021/ic401262w | Inorg. Chem. 2013, 52, 13875−13881

all RE^{3+} ions, the samarium (Sm^{3+}) ion is famous for generating intense reddish orange emitting light which was ascribed to the typical transitions between the ground state and the excited state electron configuration of Sm^{3+}. So Sm^{3+} is a versatile optically active ion for various inorganic host lattices.[19−24] Owing to all the above-mentioned reasons, we want to find a perfect host which is able to create appropriate traps and generate reddish orange LPP when doped with Sm^{3+}. $Na_2CaSn_2Ge_3O_{12}$, which is a cubic $A_2B_3C_3X_{12}$-type structure with the space group of $Ia\bar{3}d$ (No. 230), has shown more attraction than sulfide or oxysulfide as host owing to its high chemical stability, environmental friendliness, and simple preparation technique. The most important point is that it also can implant other ions such as RE^{3+} ions into the host lattice to produce phosphors emitting a variety of colors.

As we all know, solid-state reaction through sintering the mixture of solid starting materials is the most popular and useful method for synthesis of polycrystalline solids in industrial applications. In this work, we have successfully prepared a series of novel Sm^{3+}-doped $Na_2CaSn_2Ge_3O_{12}$ reddish orange LPP phosphors through a conventional solid-state method in air atmosphere. The oven temperature is 1250 °C. The results show that the Sm^{3+} concentration can affect the phosphorescent properties of $Na_2CaSn_2Ge_3O_{12}$:Sm^{3+}, such as luminescence intensity and afterglow time. The effects of the doping amount of Sm^{3+} in $Na_2CaSn_2Ge_3O_{12}$ on the properties of luminescence and afterglow were discussed. The dynamical processes of the LPP were studied, and the formation mechanism of $Na_2CaSn_2Ge_3O_{12}$:Sm^{3+} LPP phosphors was also investigated.

■ EXPERIMENTAL SECTION

Sample Preparation. Powder samples with nominal composition of $Na_2Ca_{1-x}Sn_2Ge_3O_{12}$:$x$$Sm^{3+}$ (where x = 0.0, 0.2, 0.4, 0.6, 0.8, 1.0, 1.2, and 1.4 mol %, hereafter labeled as sample S_0, S_1, S_2, S_3, S_4, S_5, S_6, and S_7) are synthesized by conventional solid-state reaction. The powders of Na_2CO_3 (99.8%), $CaCO_3$ (99.0%), SnO_2 (99.8%), GeO_2 (99.999%), and Sm_2O_3 (99.99%) acted as raw materials, and the corresponding flux of 2 mol % $(NH_4)_2C_2O_4{\cdot}H_2O$ (99.5%) and 2 mol % H_3BO_3 (99.5%) were used in each sample. Stoichiometric molar ratios of the raw materials and flux were thoroughly homogenized using a wet grinding method in an agate mortar and pestle (ethanol was added as the dispersing liquid). Finally, the alumina crucible with the mixture was put into the muffle furnace and heated at 1250 °C for 5 h in air. After cooling, the products obtained were ground.

Characterization. The crystalline structures of the phosphor powders were checked by X-ray diffraction (XRD) on a RigakuD/MAX-2400 powder diffractometer using Cu Kα radiation (1.5405 Å) in a 2θ interval from 10° to 90°. The UV−vis diffuse reflectance spectra were obtained by a Varian Cary 100 UV−vis spectrophotometer (the calibrator is $BaSO_4$ powder, reflection ~100%). An Edinburgh FLS 920 combined fluorescence lifetime and steady state spectrometer with Xe 900 (450 W xenon arc lamp) as the light source was utilized to record the photoluminescence excitation (PLE) and emission (PL) spectra of powders. The decay curves were measured immediately after the samples were activated under 254 nm UV lamp for 10 min by obtaining the signal on a PR305 phosphorophotometer (Zhejiang University Sensing Instruments Co., Ltd., China). Thermoluminescent (TL) glow curves were carried out using a FJ-427A TL meter (Beijing Nuclear Instrument Factory) at the temperature range between 280 and 650 K with 1 K/s calefactive rate. The amount of all samples was fixed at 0.0020 g. The samples were irradiated by 254 nm lamp for 10 min prior to the measurements. Except for the TL measurements, the rest of the measurements were performed at room temperature.

■ RESULTS AND DISCUSSION

Crystal Structure. The structural purities of $Na_2Ca_{1-x}Sn_2Ge_3O_{12}$:$x$$Sm^{3+}$ samples were studied by the powder X-ray diffraction. Figure 1 shows the XRD patterns of S_0, S_1, S_2,

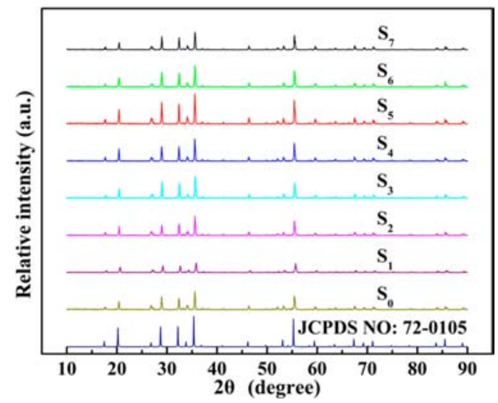

Figure 1. XRD patterns of S_0, S_1, S_2, S_3, S_4, S_5, S_6, S_7 samples and the standard data for $Na_2CaSn_2Ge_3O_{12}$ as reference.

S_3, S_4, S_5, S_6, S_7 samples and the standard data for $Na_2CaSn_2Ge_3O_{12}$ as reference. The results reveal that a predominant phase of $Na_2CaSn_2Ge_3O_{12}$ (JCPDS No. 72-0105) is presented in all powder samples and doping Sm^{3+} does not make any appreciable changes in the host structure.[25] Figure 2 represents the unit cell of the $Na_2CaSn_2Ge_3O_{12}$ host.

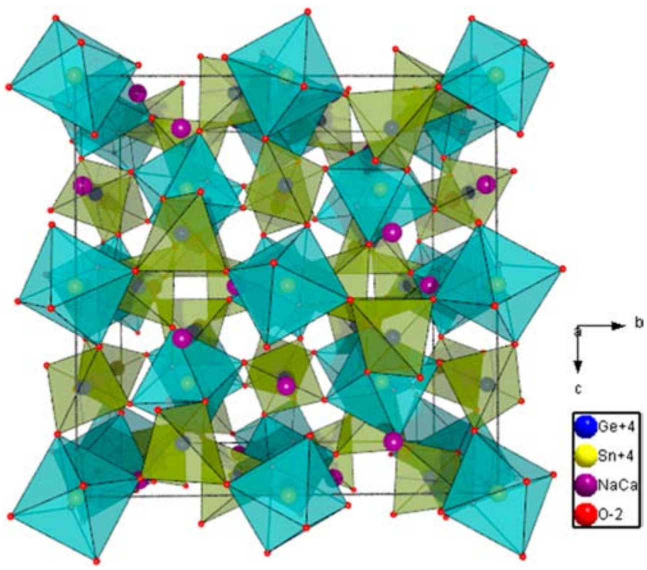

Figure 2. Schematic drawing of the crystal structure of $Na_2CaSn_2Ge_3O_{12}$.

In this unit cell, Na and Ca ions are both located at the 24c site. Sn ions are located at the 16a site. Ge ions are believed to be located at the 24d site, and O ions are located at the 96h site. The Sn site bonds to six O atoms to form an octahedron, and the Ge site is coordinated by four O atoms and forms a GeO_4 tetrahedron. Structurally $Na_2CaSn_2Ge_3O_{12}$ belongs to the cubic $A_2B_3C_3X_{12}$-type structure with the space group $Ia\bar{3}d$ (No. 230).[26] In this structure, each SnO_6 octahedron is joined to six GeO_4 tetrahedrons, each GeO_4 tetrahedron is joined to four SnO_6 octahedrons, and the octahedrons and tetrahedrons are

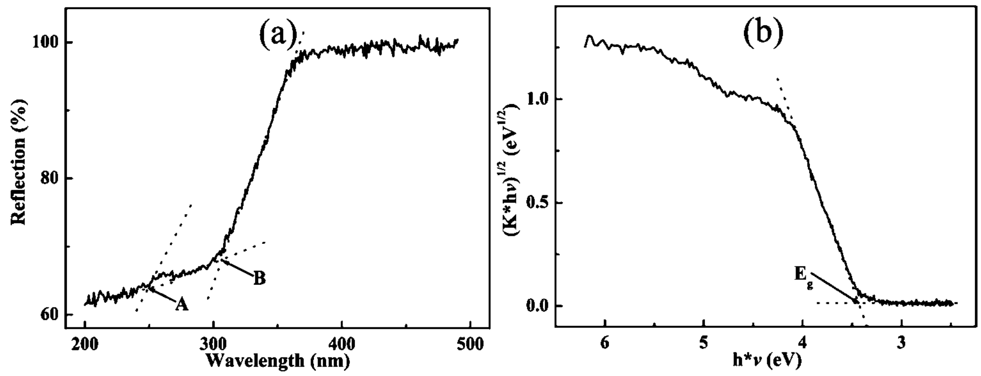

Figure 3. (a) UV−vis diffuse reflectance spectrum of undoped $Na_2CaSn_2Ge_3O_{12}$ (sample S_0), (b) relationship $(K^*h\nu)^{1/2} = f(h^*\nu)$.

connected by corner-sharing, which results in the formation of the $A_2B_3C_3X_{12}$-type skeleton. The $Na_2CaSn_2Ge_3O_{12}$ structure contains three-dimensional network of corner-sharing SnO_6 octahedrons and GeO_4 tetrahedrons; the channels in the three-dimensional network are occupied by Na cations or Ca cations. As mentioned above, the ionic positions of Na^+ and Ca^{2+} are the same. Sm^{3+} ($R_{Sm^{3+}}$ = 0.90 Å) can substitute for the Ca^{2+} ($R_{Ca^{2+}}$ = 0.94 Å) or Na^+ (R_{Na^+} = 0.96 Å) in the tetracoordinate state according to the ionic radius and valence states.

UV−Vis Diffuse Reflectance Spectra. Figure 3a shows the UV−vis diffuse reflectance spectrum of S_0 phosphor. Two band edges around 255 nm (A) and 300 nm (B) can be observed in the sample. They were known as the charge transfer transitions in the stannate[15] and the germanate host,[27,28] respectively. Relationship $(K^*h\nu)^{1/2} = f(h^*\nu)$ is shown in Figure 3b. The Kubelka−Munk transformation of diffuse reflectance data of S_0 sample is performed by the following function

$$K = \frac{(1 - R)^2}{2R} \tag{1}$$

where K is reflectance transformed according to Kubelka−Munk, h is Planck constant, ν is the light frequency, and R is reflectance (%).

The band gap (E_g) of $Na_2CaSn_2Ge_3O_{12}$, the host lattice, is estimated to be 3.43 eV.[29]

Luminescence Properties of Sm^{3+}-Doped $Na_2CaSn_2Ge_3O_{12}$. The PLE and PL spectra of a selected sample S_5 are depicted in Figure 4. The PLE spectrum (Figure 4a) was recorded by monitoring at 566 nm. It can be seen clearly that the PLE spectrum shows a strong broad band from 230 to 300 nm (maximal value positioned around 255 nm) due to host absorption and coincides precisely with the band labeled "A" appearing in the diffuse reflectance spectrum (Figure 3a). The PLE spectrum of S_5 exhibiting a strong excitation band of the host lattice in the ultraviolet (230−300 nm) region confirms the energy transfer from the host to the Sm^{3+} ions. Because Sm^{3+} ions can acquire energy from the host, the 4f → 4f intraconfigurational transitions of Sm^{3+} will appear when excited by the UV light source. So, except the band at about 230−300 nm, other bands can be observed in the 320−500 nm range with the peaks centered at 365, 404, 434, 454, 468, 473, and 482 nm corresponding to the transitions from the ground level $^6H_{5/2}$ to the excited levels $^4H_{7/2}$, $^6P_{7/2}$, $^4F_{7/2}$, $^6P_{5/2}$, $^4G_{9/2}$, $^4I_{11/2}$, and $^4I_{13/2}$ of the Sm^{3+}, respectively.[22,23] When S_5 phosphor was excited under 255 nm UV lamp, the emission spectrum (Figure 4b) was formed by four sets of lines in the reddish orange spectral region (550−720 nm) which are ascribed to the de-excitation from $^4G_{5/2}$ of Sm^{3+} to its lower multiplets of ^6H_J ($J = {}^5/_2, {}^7/_2, {}^9/_2, {}^{11}/_2$), and the $^4G_{5/2} \rightarrow {}^6H_{5/2}$ emission peak at 566 nm is the strongest one. The phenomenon of one transition featuring two emission peaks is considered to be caused by crystal field splitting. According to the selection rules,[30] the $^4G_{5/2} \rightarrow {}^6H_{5/2}$ transition mainly arising from magnetic dipole, the electric dipole mechanism played a key role in the transitions of $^4G_{5/2} \rightarrow {}^6H_J$ ($J = {}^7/_2, {}^9/_2, {}^{11}/_2$).

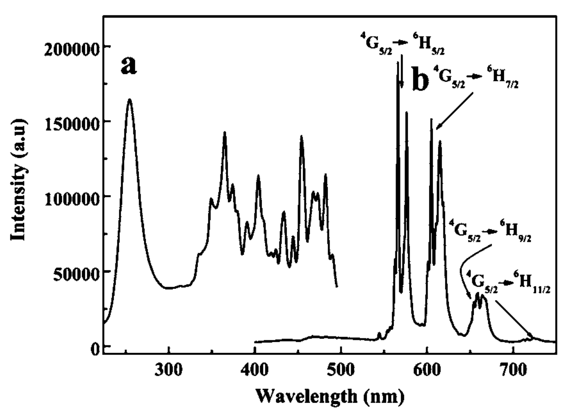

Figure 4. PLE (λ_{em} = 566 nm, a) and PL (λ_{ex} = 255 nm, b) spectra of S_5 phosphor.

To observe the effect of the doping concentration of Sm^{3+} on the luminescence intensity, we prepared a series of $Na_2CaSn_2Ge_3O_{12}$:Sm^{3+} phosphors with different concentrations of Sm^{3+}. Figure 5 shows the PL spectra of $Na_2Ca_{1-x}Sn_2Ge_3O_{12}$:$xSm^{3+}$ with different x values, and two points are worth noticing. First, the peak position and the shape of the emission spectrum are identical in different samples; second, the intensity of the emission changes with increasing concentrations of Sm^{3+}. The dependence of 566 nm emission intensity on Sm^{3+} doping concentration is presented in the inset of Figure 5. It is evident that the variation of emission intensities appears just like a part of a parabola and reaches a maximum at the values of x = 1.0%. The concentration quenching may been induced by cross relaxation processes in close Sm^{3+}−Sm^{3+}. When the Sm^{3+} concentration increases, the possibility of energy transfer between Sm^{3+} ions increases.[31] According to the report of Blasse,[32] we can roughly estimate the critical distance (the average shortest distance between the

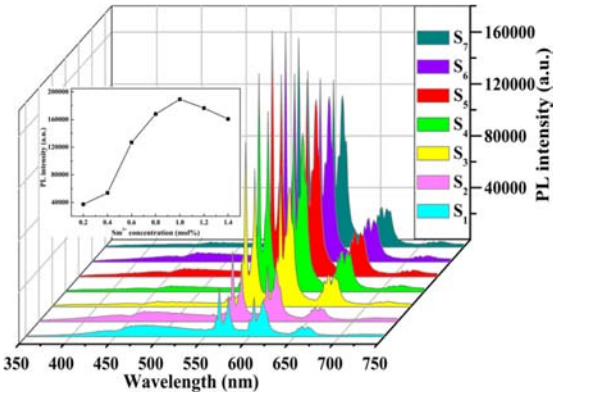

Figure 5. PL spectra of S_1, S_2, S_3, S_4, S_5, S_6, S_7 samples. The inset picture shows the intensity of 566 nm emission as a function of Sm^{3+} concentration in $Na_2Ca_{1-x}Sn_2Ge_3O_{12}$:$xSm^{3+}$ samples (λ_{ex} = 255 nm).

nearest activator ions) of energy transfer (R_c), and calculated as follows:[33−35]

$$R_c \approx 2\left(\frac{3V}{4\pi x_c N}\right)^{1/3} \tag{2}$$

Here V is the unit cell volume, x_c is the critical concentration, and N is the number of ions in a unit cell. In $Na_2CaSn_2Ge_3O_{12}$, V = 1866.6 Å^3, N = 4, and the critical concentration (x_c) is about 0.01 in our system. The R_c value is about 44.6 Å obtained by using eq 2.

Usually, the color of the phosphor can be shown by color coordinates. The chromaticity coordinates were calculated on the basis of the measured PL spectra. In this work, the chromaticity coordinates were obtained by calculation from the spectrum in Figure 4b. The chromaticity coordinates (x, y) of S_5 phosphor are (0.55, 0.40), which locates in the typical reddish orange region.

LPP Properties of $Na_2CaSn_2Ge_3O_{12}$:Sm^{3+} Phosphors. A novel reddish orange LPP phosphor family $Na_2Ca_{1-x}Sn_2Ge_3O_{12}$:$xSm^{3+}$ was discovered in our present work. The decay and fitting curves of S_5 phosphor are presented in Figure 6. It is clearly exhibited that the decay process consists of a fast decay process and a slow decay part which are well-fitted into a biexponential function as follows:

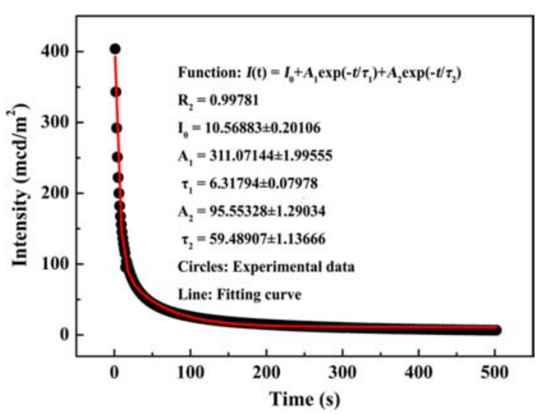

Figure 6. Afterglow decay curve (●) of S_5 phosphor (line shows the fitting result) after being activated for 10 min under 254 nm UV light.

$$I(t) = I_0 + A_1 \exp\left(\frac{-t}{\tau_1}\right) + A_2 \exp\left(\frac{-t}{\tau_2}\right) \tag{3}$$

Here, $I(t)$ and I_0 are the phosphorescence intensities at time t and 0, A_1 and A_2 are constants, t is time, and τ_1 and τ_2 are the decay times. The fitting parameters also were listed in Table 1.

Table 1. Constants (A) and Decay Times (τ) of $Na_2CaSn_2Ge_3O_{12}$:Sm^{3+} as a Function of Concentrations of Sm^{3+}

sample	A_1	A_2	τ_1 (s)	τ_2 (s)
S_1	144.1	41.7	4.5	47.8
S_2	186.7	47.9	4.6	49.3
S_3	230.8	62.7	5.0	50.1
S_4	269.1	87.1	5.8	54.3
S_5	311.0	95.5	6.3	59.5
S_6	290.2	92.9	6.0	57.4
S_7	257.0	86.1	5.5	52.6

These parameters further demonstrated that the decay processes of S_5 phosphor possessed a biexponential decay character. Initially, intensity of the afterglow decreases rapidly and then decays very slowly.[23,36] Owning to the slow decay process, the afterglow emission of the S_5 phosphor lasts for more than 4.8 h after removal of the 254 nm UV light. The decay curves (as shown in Figure 7) of all samples are in accord

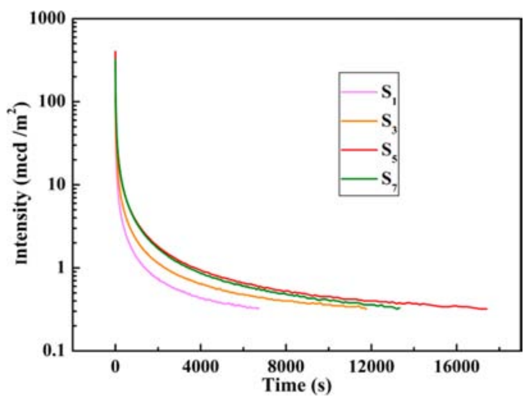

Figure 7. Afterglow decay curves of $Na_2Ca_{1-x}Sn_2Ge_3O_{12}$:$xSm^{3+}$ (x = 0.2, 0.6, 1.0, 1.4 mol %) phosphors after ceasing the 254 nm UV excitation source.

with eq 3. The obtained parameters also are listed in Table 1. It is clearly observed from Table 1 that A and τ are enhanced by the addition of Sm^{3+}. The maximum enhancement occurs in 1.0 mol % Sm^{3+} added sample. From the above results, we infer that the Sm^{3+} doping concentration in the $Na_2CaSn_2Ge_3O_{12}$ matrix can influence the afterglow properties of $Na_2CaSn_2Ge_3O_{12}$:Sm^{3+} samples. The biexponential decay model of $Na_2CaSn_2Ge_3O_{12}$:Sm^{3+} phosphor was fully consistent with the behavior of many other ions doped LPP phosphors.[37,38]

The effect of dopant concentration on the afterglow properties was evaluated by varying the concentration of Sm^{3+} in $Na_2CaSn_2Ge_3O_{12}$ samples. The decay curves of $Na_2Ca_{1-x}Sn_2Ge_3O_{12}$:$xSm^{3+}$ (x = 0.2, 0.6, 1.0, 1.4 mol %) are depicted in Figure 7. For all the curves, the decay rate of the afterglow intensity is very high at first and then become low. The Sm^{3+} quenching concentration begins with x = 1.0 mol %.

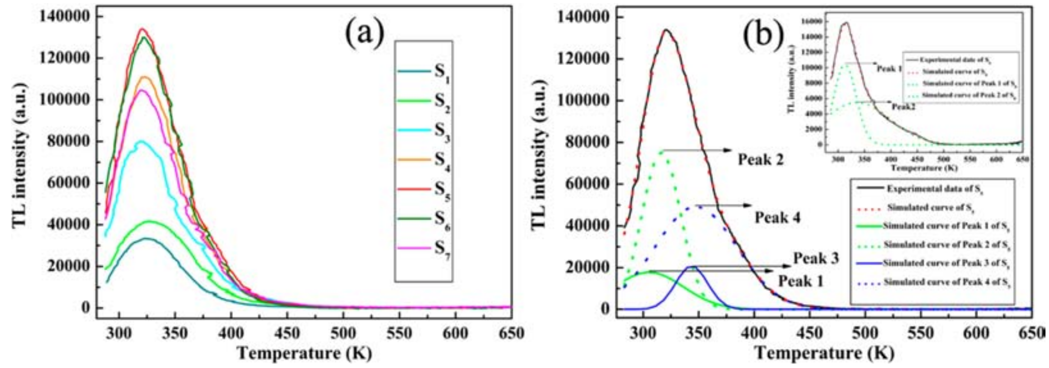

Figure 8. (a) TL curves of $Na_2Ca_{1-x}Sn_2Ge_3O_{12}$:$xSm^{3+}$ phosphors with different Sm^{3+} concentration. (b) TL curves of S_5 sample, and black solid line is the measured curve. The dotted lines and green, and blue solid lines are the simulated Gaussian curves. The insert picture of part b shows the TL curves of S_0 sample, and solid line is the measured curve. The dotted lines are the simulated Gaussian curves.

The lifetime decreased markedly from the concentration of Sm^{3+} exceeding 1.0 mol %. The results of the effect of Sm^{3+} concentration on the afterglow lifetime of $Na_2CaSn_2Ge_3O_{12}$:Sm^{3+} phosphor are in agreement with the conclusions obtained by Figure 5.

Thermoluminescence Properties. It is well-known that LPP is due to charge carriers (i.e., holes, electrons, or their pairs) which can be trapped in abundant defect (intrinsic or extrinsic) centers and then are continuously released under the action of thermostimulation.[39] The traps which were made up of the defects in the host lattice play an important role in the afterglow properties in LPP phosphors. Hence, the knowledge of the traps must be studied thoroughly in order to investigate the formation of LPP. The thermoluminescence (TL) technique is a helpful tool for evaluating the density and depth of traps generated in materials under the irradiation of UV light.[40,41] In order to study the parameters of the trapping centers produced under the excitation of ultraviolet light and further investigate the significant effect of different traps on the origin of the LPP of the $Na_2CaSn_2Ge_3O_{12}$:Sm^{3+} phosphors, the measurement of the TL glow curves of these samples was performed.

The TL curves of samples S_1−S_7 in the temperature range 280−650 K are shown in Figure 8a. Figure 8b and the insert picture of Figure 8b represent the TL curves of the S_5 and the S_0 matrix phosphors, respectively. The TL curves of the S_0 and S_5 phosphors were deconvoluted by curve fitting technique based on the Gauss equation.[42] Consequently, Chen's method[43] was used to analyze the individual deconvoluted peaks by the equation

$$E = 2.52 + 10.2(\mu_g - 0.42)\left(\frac{k_B T_m^2}{\omega}\right) - 2k_B T_m \tag{4}$$

where E is the trapping level, k_B is Boltzmann's constant, μ_g is the symmetry factor, defined as $\mu_g = \delta/\omega$, $\omega = \tau + \delta$, in which ω is the total half intensity width, τ is the left half width, and δ is the right half width. T_m is the temperature corresponding to peak intensity. The TL glow curves shown in the insert picture of Figure 8b reveal that in the S_0 matrix there are two different kinds of traps responsible for the two peaks in the TL curve situated at 311 and 343 K, respectively. At least four Gaussian curves were obtained in the TL curve of the S_5 phosphor, the peaks of the four Gaussian curves located at around 311, 318, 343, and 348 K, respectively. The values of E calculated for TL peak 1, peak 2, peak 3, and peak 4 are about 0.26, 0.55, 0.68, and 0.35 eV, respectively. The ca. 311 and 343 K TL peaks of the S_5 phosphor have not noticeably altered in comparison with that of the undoped S_0 matrix. However, two different peaks which locate at 318 and 348 K are present in the glow curve of the S_5 phosphor elucidating that doping Sm^{3+} into the $Na_2CaSn_2Ge_3O_{12}$ matrix not only enhances the trapping capacity but also creates foreign trap centers. Because the ionic positions of Na^+ and Ca^{2+} are the same and the ionic radii of Na^+ (R_{Na^+} = 0.96 Å), Ca^{2+} ($R_{Ca^{2+}}$ = 0.94 Å), and Sm^{3+} ($R_{Sm^{3+}}$ = 0.90 Å) ions are very close, the Sm^{3+} ions would chemically nonequivalently substitute the Ca^{2+} sites or the Na^+ sites when they were introduced into the $Na_2CaSn_2Ge_3O_{12}$ host matrix. The excess positive charge which was generated by Ca^{2+} or Na^+ being nonequivalently replaced by Sm^{3+} in the lattice must be compensated for in order to keep the phosphor electrically neutral. The possible approach to achieve the charge compensation of the Sm^{3+}-doped $Na_2CaSn_2Ge_3O_{12}$ phosphor is two Sm^{3+} ions substituting for three Ca^{2+} ions which result in the formation of two positive charge defects (Sm_{Ca}°) and one negative defect (V_{Ca}''), or one Sm^{3+} ion substituting for three Na^+ ions, which results in the formation of one positive charge defect ($Sm_{Na}^{\circ\circ}$) and two negative defects (V_{Na}').[15,36] The equation about the formation of defects are expressed as follows:

$$Sm_{Ca}^{\circ} + V_{Ca}'' \gg Sm_{Ca}^{x} + V_{Ca}' \tag{5}$$

$$Sm_{Na}^{\circ\circ} + V_{Na}' \gg Sm_{Na}^{\circ} + V_{Na}^{x} \tag{6}$$

The IPs of Na^+ and Ca^{2+} are 47.3 and 51.0 eV, respectively.[44] The trap depths associated with these cation vacancies would decrease in the order $Ca^{2+} > Na^+$.[45] Hence, the 311 and 343 K TL peaks are correlated with the Na^+, Ca^{2+} vacancies, respectively. This attribution has already been confirmed by the fact that these TL peaks also appeared in the $Na_2CaSn_2Ge_3O_{12}$ host as shown in the insert picture of Figure 8b. One of the commonly used methods to get excellent performance of LPP phosphors is by introducing auxiliary ions which have different valences and ionic radii compared with the host cations into the substrate.[46−48] In this work, apart from being an activator, trivalent Sm^{3+} ion can also play the role of aliovalent dopant to create defects. On the basis of the above-discussed result, the 318 and 348 K TL peaks may originate from the positive defects created by Sm^{3+} ions replacing Ca^{2+} and Na^+ ions.

Possible Mechanism of the $Na_2CaSn_2Ge_3O_{12}$:Sm^{3+} Phosphors. On the basis of the above-mentioned results, a possible mechanism was proposed to explain the generation of reddish orange LPP in $Na_2CaSn_2Ge_3O_{12}$:Sm^{3+} phosphors. So far, there is still lack of a convincing mechanism of the LPP. Nowadays the thermostimulated recombination of holes and electrons is generally accepted among all the reports about the LPP mechanism.[6,36,40,49−51] Phosphorescence mechanism of $Na_2CaSn_2Ge_3O_{12}$:Sm^{3+} can be explained as follows: part of the defects may serve as hole capture centers, while the others may serve as electron capture centers. In our present work, Sm^{3+} is an activator itself as well as the trap provider. A schematic diagram of LPP mechanism for $Na_2CaSn_2Ge_3O_{12}$:Sm^{3+} phosphors is displayed in Figure 9. The band gap of

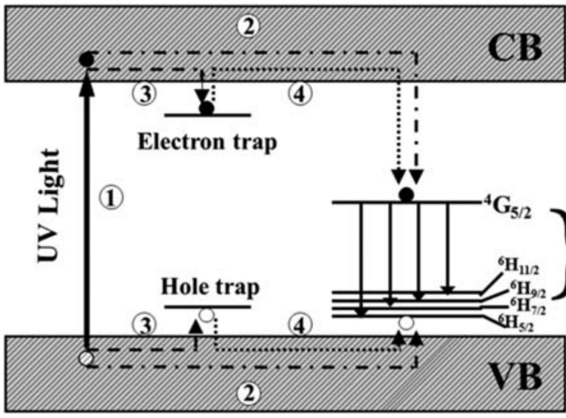

Figure 9. Schematic diagram that presents a possible trapping mechanism of the $Na_2CaSn_2Ge_3O_{12}$:Sm^{3+} phosphors. ● denotes electron trap; ○ denotes hole trap.

$Na_2CaSn_2Ge_3O_{12}$ (sample S_0) is around 3.43 eV, corresponding to the host absorption at 255 nm. We have no idea of the exact location of the Sm^{3+} levels relative to the substrate levels. Because we are only interested in the excitation, emission, and persistent luminescence process of Sm^{3+} in $Na_2CaSn_2Ge_3O_{12}$ host, the Sm^{3+} energy levels were placed in the valence and conduction band merely for explanatory purposes. Under the ultraviolet light irradiation, the valence band electrons are promoted to the conduction band, generating excited carriers (free electrons and holes) in the $Na_2CaSn_2Ge_3O_{12}$ matrix (process 1), and the luminescence centers Sm^{3+} acquired most of the excitation energy which related to the excited carries from the host through the energy transfer (process 2), and eventually generate the characteristic emissions of Sm^{3+} ions as the luminescence (process 5). However, some of the excited carriers were captured by different trapping centers through a relaxation process (process 3). After the ultraviolet light was turned off, the trapped carriers released by the thermal activation at room temperature were passed to Sm^{3+} ions through the valence band and conduction band (process 4), finally giving rise to the reddish orange light emitting LPP of Sm^{3+} because the energy transferred from the trap has a slow release ratio.

CONCLUSIONS

In conclusion, a novel reddish orange LPP phosphor Sm^{3+}-doped $Na_2CaSn_2Ge_3O_{12}$ was synthesized by conventional solid-state reaction which can last for over 4.8 h after being irradiated by 254 nm UV light. The PL spectra and the afterglow decay curves revealed that the optimum composition of phosphor was $Na_2CaSn_2Ge_3O_{12}$: 1.0 mol % Sm^{3+}. Thermoluminescence results indicated that different defects exist in all samples. The LPP is generated through the recombination of the thermally released holes and electrons which were trapped in the $Na_2CaSn_2Ge_3O_{12}$ matrix. Due to the $Na_2CaSn_2Ge_3O_{12}$:Sm^{3+} phosphors possessing numerous suitable stable traps which are able to permanently store energy at room temperature, they can serve as the storage phosphor.

ASSOCIATED CONTENT

Supporting Information

Additional experimental details, data, tables, and figures. This material is available free of charge via the Internet at http://pubs.acs.org.

AUTHOR INFORMATION

Corresponding Author

*E-mail: liuws@lzu.edu.cn. Phone: +86-931-8915151.

Notes

The authors declare no competing financial interest.

ACKNOWLEDGMENTS

The work is financially supported by the NSFC (20931003, and 91122007), the Specialized Research Fund for the Doctoral Program of Higher Education (20110211130002), and the Fundamental Research Funds for the Central Universities (lzujbky-2012-24).

REFERENCES

(1) Hölsa, J. *Electrochem. Soc. Interface* **2009**, *18*, 42−45.
(2) Luitel, H. N.; Watari, T.; Chand, R.; Torikai, T.; Yada, M.; Mizukami, H. *Mater. Sci. Eng., B* **2013**, *178*, 834.
(3) Zhang, J. C.; Yu, M. H.; Qin, Q. S.; Zhou, H. L.; Zhou, M. J. *J. Appl. Phys.* **2010**, *108*, 123518.
(4) Matsuzawa, T.; Aoki, Y.; Takeuchi, N.; Murayama, Y. *J. Electrochem. Soc.* **1996**, *143*, 2670−2673.
(5) Zhong, R. X.; Zhang, J. H.; Zhang, X.; Lu, S. Z.; Wang, X. J. *Appl. Phys. Lett.* **2006**, *88*, 201916.
(6) Liu, Y. L.; Lei, B. F.; Shi, C. S. *Chem. Mater.* **2005**, *17*, 2108−2113.
(7) Yamamoto, H.; Matsuzawa, T. *J. Lumin.* **1997**, *72*−*74*, 287−289.
(8) Lei, B. F.; Liu, Y. L.; Zhang, J. W.; Meng, J. X.; Man, S. Q.; Tan, S. Z. *J. Alloys Compd.* **2010**, *495*, 247−253.
(9) le Masne de Chermont, Q.; Chanéac, C.; Seguin, J.; Pellé, F.; Maîtrejean, S.; Jolivet, J. P.; Gourier, D.; Bessodes, M.; Scherman, D. *Proc. Natl. Acad. Sci. U.S.A.* **2007**, *104*, 9266−9271.
(10) Jia, D.; Wu, B. Q.; Zhu, J. C.A. Patent 00100388, 2000.
(11) Jia, D. D.; Zhu, J.; Wu, B. Q. *J. Electrochem. Soc.* **2000**, *147*, 386−389.
(12) Diallo, P. T.; Boutinaud, P.; Mahiou, R.; Cousseins, J. C. *Phys. Status Solidi A* **1997**, *160*, 255.
(13) Murazaki, Y.; Arai, K.; Ichinomiya, K. *Rare Earth* **2000**, *36*, 146.
(14) Fu, J. *Electrochem. Solid-State Lett.* **2000**, *3*, 350−351.
(15) Ju, Z. H.; Wei, R. P.; Zheng, J. R.; Gao, X. P.; Zhang, S. H.; Liu, W. S. *Appl. Phys. Lett.* **2011**, *98*, 121906.
(16) Lei, B. F.; Yue, S.; Zhang, Y. Z.; Liu, Y. L. *Chin. Phys. Lett.* **2010**, *27*, 037201.
(17) Zhang, J. C.; Hu, R.; Qin, Q. S.; Wang, D.; Liu, B. T.; Wen, Y.; Zhou, M. J.; Wang, Y. H. *J. Lumin.* **2012**, *132*, 2590−2594.
(18) Pan, Z. W.; Lu, Y. Y.; Liu, F. *Nat. Mater.* **2012**, *11*, 58−63.
(19) Liu, Z. Q.; Stevens-Kalceff, M.; Riesen, H. *J. Phys. Chem. C* **2012**, *116*, 8322−8331.
(20) Longo, V. M.; das Graça Sampaio Costa, M.; Zirpole Simões, A.; Rosa, I. L.; Santos, C. O.; Andrés, J.; Longo, E.; Varela, J. A. *Phys. Chem. Chem. Phys.* **2010**, *12*, 7566−7579.
(21) Liu, Y. L.; Kuang, J. Y.; Lei, B. F.; Shi, C. S. *J. Mater. Chem.* **2005**, *15*, 4025−4031.

(22) Xia, Z. G.; Chen, D. M. *J. Am. Ceram. Soc.* **2010**, *93*, 1397−1401.
(23) Lei, B. F.; Li, B.; Zhang, H. R.; Li, W. L. *Opt. Mater.* **2007**, *29*, 1491−1494.
(24) Lei, B. F.; Man, S. Q.; Liu, Y. L.; Yue, S. *Mater. Chem. Phys.* **2010**, *124*, 912−915.
(25) We cannot exactly attribute the impurities (please refer to the Supporting Information for details). The content of impurities were decreased greatly just in the absence of H_3BO_3 without changing the other experimental conditions, however, pure product was still not obtained.
(26) Durif, A.; Maupin, G. *Acta Crystallogr.* **1961**, *14*, 440−441.
(27) Li, Y. C.; Chang, Y. H.; Chang, Y. S.; Lin, Y. J.; Laing, C. H. *J. Phys. Chem. C* **2007**, *111*, 10682−10688.
(28) Poulios, D. P.; Spoonhower, J. P.; Bigelow, N. P. *J. Lumin.* **2003**, *101*, 23−33.
(29) Tauc, J.; Grigorovici, R.; Vancu, A. *Phys. Status Solidi B* **1966**, *15*, 627−637.
(30) Carnall, W. T.; Fields, P. R.; Rajnak, K. *J. Chem. Phys.* **1968**, *49*, 4412−4423.
(31) Dexter, D. L.; Schulman, J. H. *J. Chem. Phys.* **1954**, *22*, 1063−1070.
(32) Blasse, G. *Philips Res. Rep.* **1969**, *24*, 131−144.
(33) Im, W. B.; Fellows, N. N.; DenBaars, S. P.; Seshadri, R.; Kim, Y. I. *Chem. Mater.* **2009**, *21*, 2957−2966.
(34) Luo, H. D.; Liu, J.; Zheng, X.; Han, L. X.; Ren, K. X.; Yu, X. B. *J. Mater. Chem.* **2012**, *22*, 15887−15893.
(35) Hou, D. J.; Liu, C. M.; Ding, X. M.; Kuang, X. J.; Liang, H. B.; Sun, S. S.; Huang, Y.; Tao, Y. *J. Mater. Chem. C* **2013**, *1*, 493−499.
(36) Lei, B. F.; Li, B.; Zhang, H. R.; Zhang, L. M.; Cong, Y.; Li, W. L. *J. Electrochem. Soc.* **2007**, *154*, H623−H630.
(37) Liu, C. B.; Che, G. B.; Xu, Z. L.; Wang, Q. W. *J. Alloys Compd.* **2009**, *474*, 250−253.
(38) Lei, B. F.; Machida, K.; Horikawa, T.; Hanzawa, H.; Kijima, N.; Shimomura, Y.; Yamamoto, H. *J. Electrochem. Soc.* **2010**, *157*, J196−J201.
(39) McKeever, S. W. S. *Thermoluminescence of Solids*, 2nd ed.; Cambridge University Press: Cambridge, U.K., 1985.
(40) Trojan-Piegza, J.; Niittykoski, J.; Hölsä, J.; Zych, E. *Chem. Mater.* **2008**, *20*, 2252−2261.
(41) Gao, X. P.; Zhang, Z. Y.; Wang, C.; Xu, J.; Ju, Z. H.; An, Y. Q.; Liu, W. S. *J. Electrochem. Soc.* **2011**, *158*, J405−J408.
(42) Lempicki, A.; Glodo, J. *Nucl. Instrum. Methods Phys. Res., Sect. A* **1998**, *416*, 333−344.
(43) Chen, R. *J. Electrochem. Soc.* **1969**, *116*, 1254−1257.
(44) Emsley, J. *The Elements*; Clarendon Press: Oxford, U.K., 1991.
(45) Clabau, F.; Rocquefelte, X.; Le Mercier, T.; Deniard, P.; Jobic, S.; Whangbo, M.-H. *Chem. Mater.* **2006**, *18*, 3212−3220.
(46) Lin, Y. H.; Tang, Z. L.; Zhang, Z. T.; Nan, C. W. *Appl. Phys. Lett.* **2002**, *81*, 996.
(47) Cheng, B. C.; Fang, L. T.; Zhang, Z. D.; Xiao, Y. H.; Lei, S. J. *J. Phys. Chem. C* **2011**, *115*, 1708−1731.
(48) Maldiney, T.; Lecointre, A.; Viana, B.; Bessière, A.; Bessodes, M.; Gourier, D.; Richard, C.; Scherman, D. *J. Am. Chem. Soc.* **2011**, *133*, 11810−11815.
(49) Qiu, J. R.; Miura, K.; Inouye, H.; Fujiwara, S.; Mitsuyu, T.; Hirao, K. *J. Non-Cryst. Solids* **1999**, *244*, 185−188.
(50) Clabau, F.; Rocquefelte, X.; Jobic, S.; Deniard, P.; Whangbo, M.-H.; Garcia, A.; Le Mercier, T. *Chem. Mater.* **2005**, *17*, 3904−3912.
(51) Lei, B. F.; Zhang, H. R.; Mai, W. J.; Yue, S.; Liu, Y. L.; Man, S. Q. *Solid State Sci.* **2011**, *13*, 525−528.